Supporting Information

Requist et al. 10.1073/pnas.1322239111

SI Text

First-Principles Electronic Structure Calculations. Density functional theory calculations of nitric oxide (NO) adsorption were performed using the slab method with three to seven gold layers and a 3×3 hexagonal supercell of the unreconstructed Au(111) surface, corresponding to 1/9 monolayer coverage. This cell was large enough to reduce the interaction between periodic images of the NO molecule to a negligible level. Selected calculations were repeated with 2×2, $2\sqrt{3}\times\sqrt{3}$, and $2\sqrt{3}\times2\sqrt{3}$ cells to verify convergence. The unreconstructed Au(111) surface is expected to be a good approximation to the face-centered cubic (fcc) regions of the well-known $22\times\sqrt{3}$ "herringbone" reconstruction, where the experimental measurements were performed. For calculations of the adsorption energy, the vacuum layer was set to 16.9 Å, whereas for calculations of the scattering phase shifts, it was reduced to 8.4 Å, corresponding to the experimental tip height. The latter value was large enough that the shape of the tip (Fig. 1 of the main text) had a negligible effect on the adsorption geometry and hybridization linewidths. Hence, the scattering calculations were performed without any model for the tip, essentially using the bottom of the slab as a broad distant probe.

The unreconstructed Au(111) surface presents four distinct high-symmetry adsorption sites—fcc, hexagonal close packed (hcp), bridge, and on top. For each site, all of the coordinates of NO and the two highest layers of gold were fully optimized. By subsequently applying constraints to the Au atoms, it was found that only the relaxation of the Au atoms nearest to N had a significant effect on the results, and therefore in the scattering calculations we fixed all Au atoms to their bulk positions, except the one, two, or three Au atoms nearest N in the case of top, bridge, and hollow site adsorption, respectively. At the top site, the Au atom directly beneath N, which we label $\mathrm{Au_{top}}$, is pulled out of the surface by 0.11 Å, enhancing the interaction between the NO $2\pi^*$ molecular orbitals and an *spd* hybrid orbital (mainly d_{z^2}) of $\mathrm{Au_{top}}$.

Table S1 summarizes our ab initio results for gas phase NO and NO/Au(111), including the adsorption energy E_{ads}, magnetic moment μ, NO bond length d_{NO}, AuN bond length d_{AuN}, the stretching frequency ν_{NO}, and electric dipole moment calculated with generalized gradient approximation (GGA)+U. The magnetic moment is reported for the entire cell, including the small induced magnetization on gold. The surface-adsorbate electric dipole moment was calculated by applying a sawtooth-shaped potential along the z direction. At the top site, NO was found to tilt away from the upright configuration, giving a $\mathrm{Au_{top}}$-N-O angle of 122.4°, in agreement with earlier calculations (1). The tilting, which accounts for a large part of the adsorption energy, is crucial for the present study because it alters the Kondo physics by lifting the degeneracy of the $2\pi^*$ orbitals. The molecule tilts toward one of the six nearest-neighbor surface gold atoms of $\mathrm{Au_{top}}$. For definiteness, we take the molecule to tilt in the positive x direction, so that the tilt plane is the xz plane. The degenerate $2\pi^*$ orbitals split into two orbitals that we label $2\pi^*_e$ and $2\pi^*_o$ according to their symmetry (even or odd) with respect to reflection through the tilt plane. Full geometry optimization shows that the tilt plane undergoes a small azimuthal rotation of 8.6° around the surface normal. The order of magnitude of the calculated adsorption energies agrees with an estimate of 400 meV from temperature-programmed desorption spectroscopy (2) and the results of a comprehensive study (1) of NO adsorption on metal surfaces, although the site dependence differs. We are not aware of any further experimental data for NO/Au (111), but our calculations of the molecule in vacuum (Table S1) are in good agreement with gas phase measurements. The calculated ionization energy of NO, 9.007 eV, is also fairly close to the experimental value 9.27483 ± 0.00005 eV (3). The work function of gold, calculated with a 24-layer slab with 24 Å of vacuum, is 5.19 eV and compares favorably with the experimental value 5.31 eV (3).

In view of the weak adsorption energy, selected calculations were performed with the following four functionals to judge the sensitivity of the results to the choice of exchange-correlation functional: (*i*) the local (spin) density approximation (LDA) of Perdew and Zunger (5), (*ii*) the GGA of Perdew et al. (6), (*iii*) the Heyd–Scuseria–Ernzerhof (HSE) hybrid functional (7), and (*iv*) a modified version (8) of the Vydrov–Van Voorhis (VV10) functional (9) describing van der Waals interactions. The LDA approximation, known to be overbonding for molecules on surfaces, was found to be inadequate, causing NO to demagnetize. The VV10 functional increased the adsorption energy uniformly for all sites, yielding 540 meV, 380 meV, and 360 meV for the on-top, bridge, and fcc sites, respectively. Hybrid functionals have been found to give good results for the adsorption of small molecules on metal surfaces (10); however, because they open a small gap at the Fermi energy in metals, they are potentially problematic when the molecular levels lie close to the Fermi energy, as they do in our case. Moreover, such a gap would cause artifacts in the calculation of the scattering phase shifts. For these reasons, all of the results reported in the main text were obtained with the GGA and GGA+U.

Hubbard interactions $U_{\mathrm{N}}=U_{\mathrm{O}}=1$ eV were applied to the N and O p orbitals in the GGA+U scheme to stabilize the magnetic moment. Similar values have been used for CO to correct the adsorption site preference on Pt(111) (11) and Cu(111) and Cu (001) (12). We also used Hubbard interactions to correct the energy of the Au d bands, which in LDA and GGA (13, 14) is too high compared with that in angle-resolved photoemission spectroscopy (15). We found that the value $U_{\mathrm{Au}}=1.5$ eV shifts the fully occupied d bands down rigidly by 0.5 eV, bringing them into agreement with experiment and leaving the *sp* bands virtually unchanged. This value of U_{Au} was adopted in calculating all quantities in Table S1. The GGA+U scheme has been used in a similar way to correct the d states of Ni in a study of the adsorption of CO and NO/NiO(100) (16, 17).

The projected densities of states for the isolated molecule, the clean surface, and the combined surface–adsorbate system are shown in Fig. S2. The most important observation is that the degeneracy of the $2\pi^*_e$ and Γ_o orbitals is broken by the tilting of the molecule, yet both remain partially occupied. The tilting of the molecule away from the upright configuration increases the hybridization of the $2\pi^*_e$ orbital and decreases the hybridization of the $2\pi^*_o$ orbital. As reported in Table S2, the hybridization Γ_e becomes fives times as large as Γ_o for the optimal tilt angle of nearly 60°.

Despite the substantial tilting of the molecule, there is only a relatively weak symmetry breaking in the $2\pi^*$ orbital occupations. One might have expected the $2\pi^*_e$ orbital to be nearly empty, because its bare energy is pushed up by as much as 0.24 eV due to its antibonding interaction with the *spd* hybrid orbital of $\mathrm{Au_{top}}$. Instead, it is even more occupied than the $2\pi^*_o$ orbital. The $2\pi^*_e$ and $2\pi^*_o$ molecular orbitals have fractional occupation numbers, $n_e=0.65$ and $n_o=0.44$, adding up to slightly more than 1, consistent with modest charge transfer from the surface to the molecule. The degeneracy of the 1π orbitals is also lifted by the

tilting, but they split in the opposite direction because they lie below rather than above the d states in energy. The lack of distinct symmetry breaking in the $2\pi^*$ orbital occupations might be a spurious result, possibly caused by self-interaction error, or it might be a genuine consequence of orbital fluctuations. Hubbard interactions in nitrogen and oxygen are unable to induce a stronger symmetry breaking even though they increase the $2\pi_e^*/2\pi_o^*$ splitting for the spin and orbital symmetry-broken solution in vacuum. It might be possible to achieve orbital symmetry breaking by applying Hubbard-type interactions to molecular orbitals rather than atomic orbitals (*cf.* ref. 11) or in an approach with inherently less self-interaction error such as reduced density matrix functional theory, but we do not pursue these approaches here.

The Blyholder (18) and Hammer–Morikawa–Norskov (19) models, which describe the adsorption of CO on metals in terms of σ donation and π back bonding, provide a starting point for understanding the bonding interactions between NO and the gold surface; however, σ and π are no longer proper symmetries due to the tilting of the molecular axis. Modest back-bonding interactions are visible at the top of the d band (~2.5 eV below the Fermi energy) in Fig. S2, coinciding with peaks in the $\mathrm{Au_{top}}$ d_{z^2} states. The strong participation of the $\mathrm{Au_{top}}$ d_{z^2} states in the $2\pi_e^*$, 5σ, $1\pi_e$, and 4σ molecular resonances is an important feature of the bonding interaction. There are important differences between the adsorption of NO and that of CO on noble metals, because NO is an open-shell molecule.

Constructing an Anderson Impurity Model. An Anderson model representing the hybridization of the $2\pi^*$ molecular orbitals of NO with the Au(111) surface is defined in Eq. **1** of the main text. In specifying the interaction Hamiltonian H_{int}, it is convenient to start from the molecule in vacuum. Because the isolated molecule has cylindrical symmetry, the interactions in the $2\pi^*$ sector depend on only two independent parameters and can be expressed as

$$H_{int} = \frac{V}{2}N(N-1) - 2J\mathbf{S}^2 + \frac{J}{2}L_z^2, \qquad \textbf{[S1]}$$

where N is the total number of electrons, $\mathbf{S}$ is the total spin operator, and L_z is the total z component of angular momentum. The two degenerate $2\pi^*$ states, formed from the p_x and p_y orbitals of N and O, can be chosen to be eigenstates of L_z; i.e., $|m=\pm 1\rangle$. The $|m=0\rangle$ state is not considered because the p_z orbitals, being involved in σ bonding, are far lower (~7.5 eV) in energy. Because we are considering the symmetry breaking caused by tilting, we express Eq. **S1** in terms of the $2\pi_x^*$ and $2\pi_y^*$ states, which have nodes in the yz and xz planes, respectively. Using the relations $c_{m=1} = (-c_x - ic_y)/\sqrt{2}$ and $c_{m=-1} = (c_x - ic_y)/\sqrt{2}$, we find

$$H_{int} = U_x n_{x\uparrow} n_{x\downarrow} + U_y n_{y\uparrow} n_{y\downarrow} + U_{xy} n_x n_y + J_H \mathbf{S}_x \cdot \mathbf{S}_y + W + \beta N, \qquad \textbf{[S2]}$$

where the U terms are on-site and intersite Hubbard interactions, the J_H term is a Hund interaction ($\mathbf{S}_\alpha$ is the spin operator for the $2\pi_\alpha^*$ state, not the α-component of spin), and W is a double hopping term $W = W_{xy} c_{x\uparrow}^\dagger c_{x\downarrow}^\dagger c_{y\downarrow} c_{y\uparrow} + W_{xy} c_{y\uparrow}^\dagger c_{y\downarrow}^\dagger c_{x\downarrow} c_{x\uparrow}$. The parameters are uniquely determined by (V,J) according to the formulas $U_x = U_y = V + 3J$, $U_{xy} = V - J/2$, $J_H = -6J$, $W_{xy} = -J$, and $\beta = -J/2$.

When the molecule is brought down to the surface in an upright configuration at the on-top, fcc, or hcp sites, the crystal field lowers the cylindrical symmetry to C_{3v} symmetry. The degeneracy of the $2\pi^*$ states is preserved and Eqs. **S1** and **S2** remain exact. The tilting of the molecule breaks the symmetry and lifts the $2\pi^*$ degeneracy. The $2\pi_x^*$ orbital evolves into the even $2\pi_e^*$ orbital (Fig. 2 of the main text) that hybridizes strongly with the surface. The $2\pi_y^*$ orbital becomes the odd $2\pi_o^*$ orbital with much weaker hybridization. Eq. **S2** remains a valid description of interactions in the $2\pi^*$ sector; however, because the $2\pi_e^*$ and $2\pi_o^*$ orbitals are hybridized with the surface, the interaction parameters will no longer have exactly the same relationship with (V,J) that they have in cylindrical symmetry.

For tilted NO at the on-top site, there were not enough ab initio data to fit all of the parameters in Eq. **S2**, so we have taken the following strategy. We have fitted the parameters that are most sensitive to the tilting, namely ϵ_α and U_α, by matching the spin-symmetry broken mean-field $\epsilon_{\alpha\sigma}$ of the Anderson model to $\epsilon_{\alpha\sigma}^{DFT}$ inferred from the resonances in the ab initio phase shifts. The hybridization linewidths $2\Gamma_\alpha$ were calculated by fitting the resonances in the scattering phase shifts to the functional form

$$\eta_{\alpha\sigma}(\epsilon) = \frac{\pi}{2} + \arctan\frac{\epsilon - \epsilon_{\alpha\sigma}}{\Gamma_\alpha} + \delta_\alpha, \qquad \textbf{[S3]}$$

where δ_α is a constant shift attributable to potential scattering. An example of the fitting is shown in Fig. S1. The Hund interaction J_H was set equal to its value for gas phase NO, and the remaining parameters U_{eo} and W_{eo} were assumed to have the same relationship to V and J that they have in cylindrical symmetry (as in gas phase). In this way, all model parameters can be fitted reliably, and we obtain the results in Table S2.

For upright NO at the bridge site, the symmetry is lowered to C_{2v}. The $2\pi_{e/o}^*$ state is defined to be the state that is even/odd with respect to the plane containing NO and the two nearest-neighbor Au atoms. The interaction parameters were approximated the same way as for the on-top site.

Symmetry between the $2\pi_{x/y}^*$ states is preserved for upright NO at the fcc site. The interaction parameters were approximated the same way as for the on-top site; however, because the occupied (majority spin) level $\epsilon_{\alpha\uparrow}^{DFT}$ is degenerate and therefore pinned to the Fermi energy, we obtained a more stable fit for ϵ_α by requiring charge consistency between density functional theory (DFT) and numerical renormalization group (NRG); i.e., $n_\alpha^{DFT} = n_\alpha^{NRG}$.

Scanning Tunneling Spectroscopy. The densities of states measured with a clean Au tip over NO molecules and over the clean Au (111) surface several nanometers away from the molecules are shown in Fig. S3 for an extended energy range around the Fermi energy. The step at about −0.45 eV on the gold surface marks the bottom of the surface state band (20). The surface states cannot be detected on top of the NO molecules and gradually vanish when the tip approaches the molecules. The only sharp feature in the NO spectrum above the noise level is the zero-bias dip. The broad and weak bumps at about −0.15 eV and 0.3 eV approximately coincide with the shoulders of the spectral functions of Fig. 3*F* of the main text.

1. Gajdos M, Hafner J, Eichler A (2006) Ab initio density-functional study of NO on close-packed transition metal and noble metal surfaces: I. molecular adsorption. *J Phys Condens Matter* 18:13–40.
2. Nakamoto K (1986) *Infrared and Raman Spectra of Inorganic and Coordination Compounds* (Wiley, New York).
3. Hoy AR, Johns JWC, McKellar ARW (1975) Stark spectroscopy with the CO laser: Dipole moments, hyperfine structure, and level crossing effects in the fundamental band of NO. *Can J Phys/Rev Can Phys* 53:2029–2039.
4. McClure SM, Kim TS, Stiehl JD, Tanaka PL, Mullins CB (2004) Adsorption and reaction of nitric oxide with atomic oxygen covered Au(111). *J Phys Chem B* 108: 17952.
5. Reiser G, Habenicht W, Müller-Dethlefs K, Schlag EW (1988) The ionization energy of nitric oxide. *Chem Phys Lett* 152:119–123.
6. Michaelson HB (1977) The work function of the elements and its periodicity. *J Appl Phys* 48:4729–4733.
7. Perdew JP, Zunger A (1981) *Phys Rev B* 23:5048–5079.

8. Perdew JP, Burke K, Ernzerhof M (1996) Generalized gradient approximation made simple. *Phys Rev Lett* 77(18):3865–3868.
9. Heyd J, Scuseria GE, Ernzerhof M (2003) Hybrid functionals based on a screened Coulomb potential. *J Chem Phys* 118:8207–8215.
10. Sabatini R, Gorni T, de Gironcoli S (2013) Nonlocal van der Waals density functional made simple and efficient. *Phys Rev B* 87:041108.
11. Vydrov OA, Van Voorhis T (2010) Nonlocal van der Waals density functional: the simpler the better. *J Chem Phys* 133(24):244103.
12. Wang Y, de Gironcoli S, Hush NS, Reimers JR (2007) Successful a priori modeling of CO adsorption on Pt(111) using periodic hybrid density functional theory. *J Am Chem Soc* 129(34):10402–10407.
13. Kresse G, Gil A, Sautet P (2003) Significance of single-electron energies for the description of CO on Pt(111). *Phys Rev B* 68:073401.
14. Gajdos M, Hafner J (2005) CO adsorption on Cu(111) and Cu(001) surfaces: Improving site preference in DFT calculations. *Surf Sci* 590:117–126.
15. Takeuchi N, Chan CT, Ho KM (1991) Au(111): A theoretical study of the surface reconstruction and the surface electronic structure. *Phys Rev B* 43(17):13899–13906.
16. Mazzarello R, Dal Corso A, Tosatti E (2008) Spin-orbit modifications and splittings of deep surface states on clean Au(111). *Surf Sci* 602:893–905.
17. Kevan SD, Gaylord RH (1987) High-resolution photoemission study of the electronic structure of the noble-metal (111) surfaces. *Phys Rev B* 36(11):5809–5818.
18. Rohrbach A, Hafner J, Kresse G (2004) Molecular adsorption on the surface of strongly correlated transition-metal oxides: A case study for CO/NiO(100). *Phys Rev B* 69: 075413.
19. Rohrbach A, Hafner J (2005) Molecular adsorption of NO on NiO(100): DFT and DFT+U calculations. *Phys Rev B* 71:045405.
20. Blyholder G (1964) Molecular orbital view of chemisorbed carbon monoxide. *J Phys Chem* 68:2772–2777.
21. Hammer B, Morikawa Y, Norskov JK (1996) CO chemisorption at metal surfaces and overlayers. *Phys Rev Lett* 76(12):2141–2144.
22. Chen W, Madhavan V, Jamneala T, Crommie MF (1999) Scanning tunneling microscopy observation of an electronic superlattice at the surface of clean gold. *Phys Rev Lett* 80(7):1469–1472.

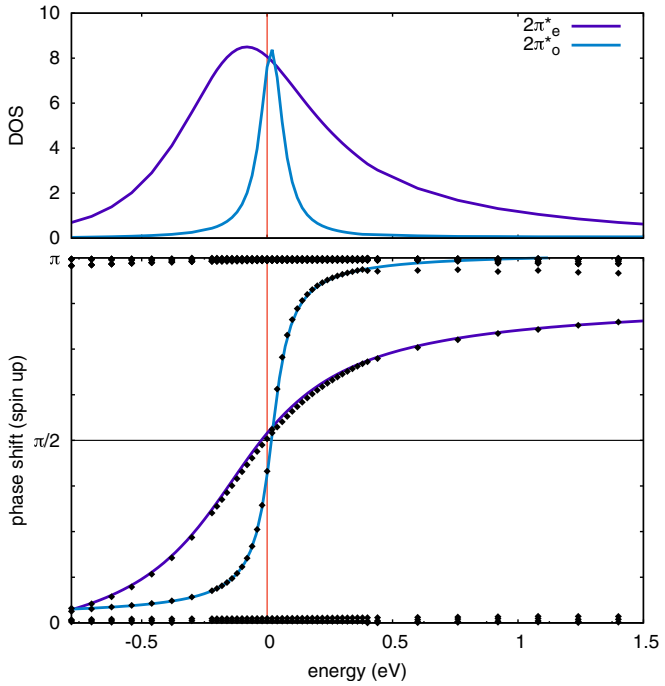

Fig. S1. Examples of resonances in the scattering phase shifts with fits to Eq. **S3** (*Lower*) and corresponding peaks in the density of states (DOS) (*Upper*).

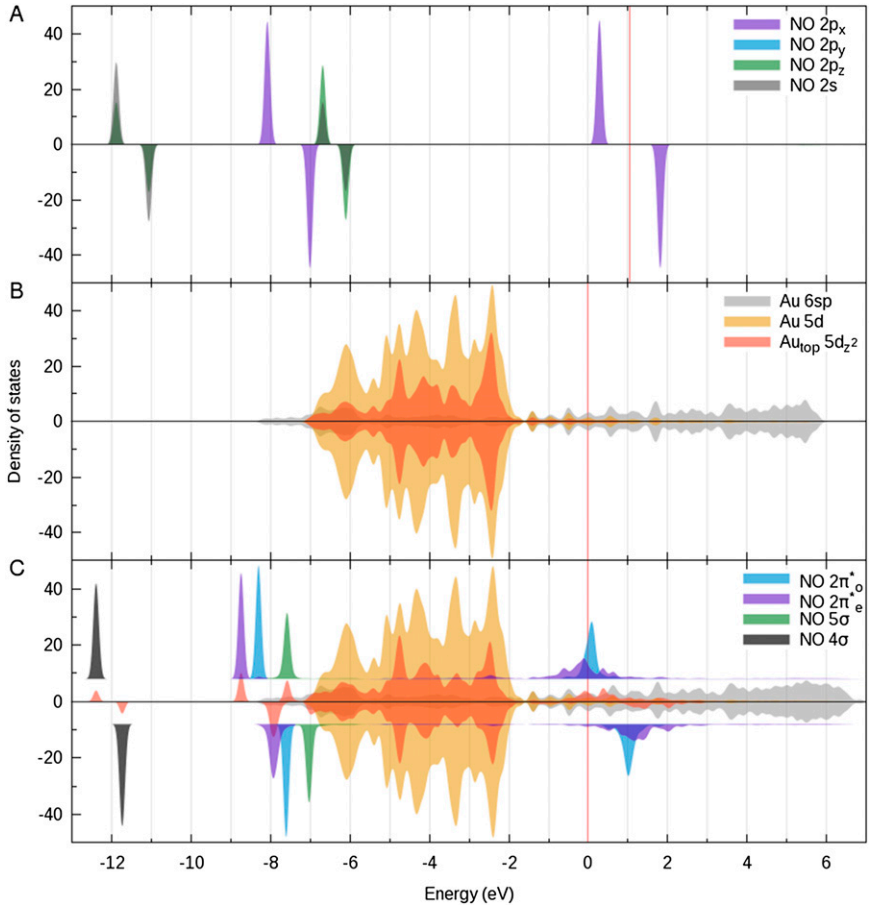

Fig. S2. (*A*–*C*) Projected density of states of (*A*) gas phase NO, (*B*) three-layer Au(111) slab, and (*C*) NO/Au(111) slab system. Energies have been shifted to align the vacuum levels of all systems; vertical red lines indicate the respective Fermi energies. Artificial Gaussian broadening of 0.10 eV is used. NO $2p_x$ and $2p_y$ orbitals are degenerate in gas phase. The densities of states of the $2\pi^*$ orbitals are calculated from weighted sums of N and O p_x and p_z orbitals, corresponding to the tilting.

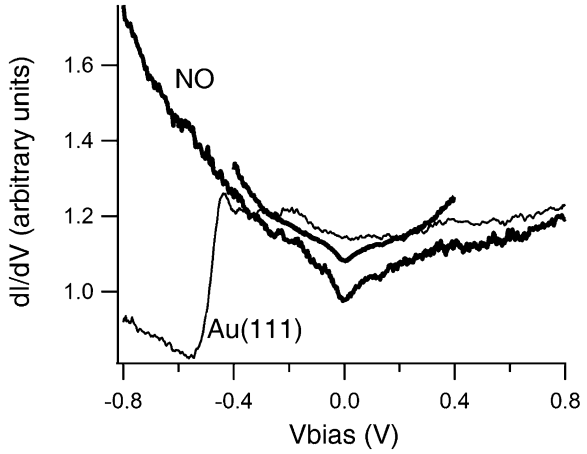

Fig. S3. STS spectra taken over NO molecules at 70 K (thick lines) and over the clean Au(111) surface a few nanometers away at 5 K (thin line).

Table S1. Ab initio properties of gas phase NO and NO/Au(111)

Site	Configuration	E_{ads} (eV)	μ, μ_B	d_{NO}, Å	d_{AuN}, Å	ν_{NO}, cm^{-1}	Electric dipole, D
Gas phase	—	—	1.00	1.1662 (1.148)*	—	1,885 (1,903)*	0.109 (0.157)†
On top	Tilted	0.320	0.89	1.1704	2.3309	—	0.353
Bridge‡	Vertical	0.148	0.94	1.1653	2.8206	—	0.313
fcc‡	Vertical	0.122	1.14	1.1688	2.8576	—	0.172

*Experiment, ref. 1.
†Experiment, ref. 2.
‡Metastable configuration.

1. Nakamoto K (1986) *Infrared and Raman Spectra of Inorganic and Coordination Compounds* (Wiley, New York).
2. Hoy AR, Johns JWC, McKellar ARW (1975) Stark spectroscopy with the CO laser: Dipole moments, hyperfine structure, and level crossing effects in the fundamental band of NO. *Can J Phys/Rev Can Phys* 53:2029–2039.

Table S2. Anderson model parameters for NO/Au(111)

Site	ϵ_e	ϵ_o	Γ_e	Γ_o	U_e	U_o	U_{eo}	J_H	W_{eo}
On top	−0.92	−1.02	0.33	0.068	2.24	2.04	1.67	−0.807	−0.134
Bridge	−1.22	−1.83	0.12	0.13	2.01	3.18	2.13	−0.807	−0.134
fcc	−1.00	−1.00	0.22	0.22	2.45	2.45	1.83	−1.06	−0.178

All quantities are in electronvolts; SDs of ϵ_e, ϵ_o, Γ_e, and Γ_o for the on-top site are 0.04, 0.01, 0.036, and 0.015, respectively.